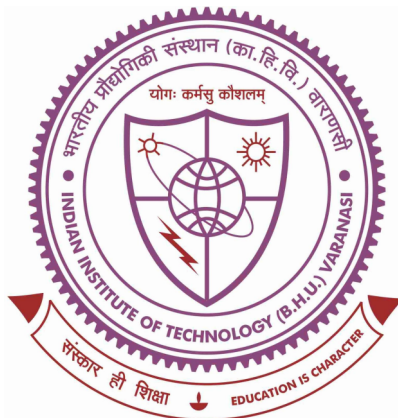


Tuning Charge Transfer Dynamics in Halide Perovskites for Improved Photoredox Organic Reactions



Thesis submitted in partial fulfillment for the
Award of Degree

Doctor of Philosophy

By

Vishesh Kumar

DEPARTMENT OF CHEMISTRY
INDIAN INSTITUTE OF TECHNOLOGY
(BANARAS HINDU UNIVERSITY)
VARANASI - 221005
INDIA

Roll No. 19051505

Year 2025

**DEDICATED TO MY LOVING
PARENTS...**

CERTIFICATE

It is certified that the work contained in the thesis titled “**Tuning Charge Transfer Dynamics in Halide Perovskites for Improved Photoredox Organic Reactions**” by Vishesh Kumar has been carried out under my supervision, and this work has not been submitted elsewhere for a degree.

It is further certified that the student has fulfilled all the requirements of the Comprehensive Examination, Candidacy, and SOTA for the award of the Ph.D. degree.

Dr. Arindam Indra
Associate Professor
Department of Chemistry
IIT (BHU) Varanasi
UP-221005



Dr. Arindam Indra

(Supervisor)

**Department of Chemistry,
Indian Institute of Technology
(Banaras Hindu University),
Varanasi-221005**

Date: 07/10/25
Place: Varanasi

DECLARATION BY THE CANDIDATE

I, "Vishesh Kumar", certify that the work embodied in this thesis is my own bonafide work and carried out by me under the supervision of "Dr. Arindam Indra" from "December 2019" to "July-2025," at the Department of Chemistry, Indian Institute of Technology, (BHU), Varanasi. The matter embodied in this thesis has not been submitted for the award of any other degree/diploma. I declare that I have faithfully acknowledged and given credit to the research workers wherever their works have been cited in my work in this thesis. I further declare that I have not will fully copied any other's work, paragraphs, text, data, results, etc., reported in journals, books, magazines, reports dissertations, theses, etc., or available at websites and have not included them in this thesis and have not cited as my own work.

Date: 07/10/25

Place: Varanasi

Vishesh Kumar
(Vishesh Kumar)

CERTIFICATE BY THE SUPERVISOR

It is certified that the above statement made by the student is correct to the best of my/our knowledge.


Supervisor
Dr. Arindam Indra
Associate Professor
Department of Chemistry
IIT (BHU) Varanasi
UP-221005

Dr. Arindam Indra
Department of Chemistry
Indian Institute of Technology
(Banaras Hindu University)
Varanasi- 221005


Head of Department

Prof. Sundaram Singh
विभागाध्यक्ष / HEAD
Department of Chemistry,
Department of Chemistry
Indian Institute of Technology
भारतीय प्रौद्योगिकी संस्थान (का. वि. प्रौ. वि.)
(Banaras Hindu University),
Varanasi-221005

COPYRIGHT TRANSFER CERTIFICATE

Title of the Thesis: **Tuning Charge Transfer Dynamics in Halide Perovskites for Improved Photoredox Organic Reactions.**

Name of the Student: **Vishesh Kumar**

COPYRIGHT TRANSFER

The undersigned hereby assigns to the Indian Institute of Technology (Banaras Hindu University), Varanasi, all rights under copyright that may exist in and for the above thesis submitted for the award of the "**Doctor of Philosophy**" degree.

Date: 07/10/25

Place: Varanasi.

Vishesh Kumar

(Vishesh Kumar)

Note: However, the author may reproduce or authorize others to reproduce material extracted verbatim from the thesis or derivative of the thesis for the author's personal use, provided that the source and the Institute's copyright notice are indicated.

Acknowledgement

It is indeed my proud privilege to express my deep sense of gratitude and indebtedness to my supervisor, Dr. Arindam Indra, Department of Chemistry, Indian Institute of Technology (BHU), Varanasi, for his enormous help, cooperation, and valuable supervision that he has extended to me for the successful completion of this investigation. I am indebted to him for his consistent encouragement, sustained interest, and parental care throughout the research period.

I am obliged very much to express my sincere thanks to HOD, Prof. Sundaram Singh, and Ex-HOD, Prof. Y. C. Sharma, Department of Chemistry, IIT (BHU), for providing necessary facilities and constant motivation throughout my research work.

It is my pleasure to express my cheers to all RPEC members, Dr. P. Makam, Department of Chemistry, IIT (BHU), and Dr. S. K. Jain, Department of Pharmaceutical Engineering and Technology, IIT (BHU) Varanasi, for their valuable suggestions, constant guidance, and kind encouragement during my research work. Also, I would like to acknowledge Prof. E.S.S. Iyer (IIT Goa) and Prof. K. Kailasam (INST Mohali) for Femtosecond transient spectroscopy and EPR characterization. They always came forward to assist me whenever I needed.

My passionate thanks go to all the faculty members of the Department of Chemistry, IIT (BHU), for their support and encouragement.

I constraint special thanks to all non-teaching staff (Mr. Rambish, Neeraj, Abhishek, and Amit) of the Department of Chemistry, IIT (BHU), as this work would have never been completed without their technical support.

I also gratefully acknowledge to the Council of Scientific and Industrial Research (CSIR), Anushandhan Bhavan, New Delhi, for the financial support in the form of JRF and SRF.

I gratefully acknowledge the facilities provided by CIFC, IIT (BHU), Varanasi, for doing various characterizations of samples.

I am blessed to have very supportive and caring lab mates, Dr. Ved Vyas, Mr. Deepak Kumar, Mr. Toufik Ansari, Mr. Abhimanyu Yadav, Dr. Priyanka Maurya, Mr. Vijay Patel, Mr. Deepak Kumar Roy,

Mr. Harshit Gupta, Dr. Baghendra Singh and Mr. Ajit Kumar Singh, for their valuable support and encouragement towards the successful completion of my research work.

I am deeply gratified to express my sincere thanks to my supportive friends for their encouragement and valuable suggestions during my research work.

I would like to thank my friends and seniors "Mr. Neeraj Kumar, Mr. Deepak Kumar, Ms. Nivedita Singh, Mr. Anjani Kumar, Dr. Ashish Kumar Kushwaha, Mr. Abhay Narayan Mishra, Mr. Asheesh Kumar Yadav, Mr. Arif Mondal, Mr. Satendra Kumar, Mr. Amar Nath, Mr. Ramu Singh, Mr. Raghuvccer, Mr. Birendra Kumar, Mr. Satyasen Yadav, Mr. Ramanujan Singh, Mr. Tarun Kumar, Mr. Ajay Pratap, Dhirendra Yadav, Dr. Nitin Kumar, Dr. Dinesh Prajapati, and" for their help and support.

I would like to my deepest affection to my loving Father "Ram Vishal", caring mother "Bittan Devi," and sister "Manita Devi, Manisha Kumari," brothers "Birendra Kumar, Mahendra Kumar, Vishrendra Kumar" and all my family members for their love, concern, continuous moral support and encouragement which enabled me to perform my liabilities.

I am also grateful to my cousin brothers "Dinesh Kumar, Vishvendra Nath, Phool Chang, and Vishved Bahadur" for their motivation, support, and encouragement.

My special thanks to my teachers, "Mr. Rahul Kesharwani, Birendra Pandey, and Narendra Pandey" for their support and encouragement in the entire research period.

At the last but not the least, I thank to all my well-wishers and critics whose names I may have failed to mention here unintentionally. Thanks to all of you for being there for me when times were the toughest.

Date: 09/07/2025

Place: Varanasi

Vishesh Kumar
(Vishesh Kumar)

List of Figures

Figure No.	Title	Page No.
Figure 1.1	Steps in the photocatalytic reaction process. (i) Light absorption generates electron–hole pairs. (ii) Excited charge carriers (electrons and holes) separate. (iii) Electrons and holes migrate to the photocatalyst surface. (iii) Competing process: charge recombination. (iv) Surface charges drive redox reactions (R: reduction, O: oxidation)	3
Figure 1.2	Reactive oxygen species (ROS) are produced during the photocatalytic reduction of oxygen and water oxidation. Left: redox potentials of various ROS. These species possess suitable oxidative power and play a key role in the selective oxidation of organic feedstocks into high-value-added chemicals.	4
Figure 1.3	(a) Roles of cocatalysts in photocatalytic reactions. (b) Schematic representation of different types of cocatalysts involved in photocatalytic reduction and oxidation processes.	6
Figure 1.4	Energy band configurations of various heterojunction photocatalysts include: (a) Type-I (straddling gap), (b) Type-II (staggered gap), (c) Type-III (broken gap), and (d) Z-scheme systems. (e) Illustration of charge separation dynamics in a Z-scheme heterojunction showing: A) the individual semiconductor energy levels before physical contact, B) band alignment upon contact in the absence of light, and C) charge transfer behavior under light irradiation as the system reaches equilibrium.	8
Figure 1.5	Structure, phase transformation, and cation transmutation in double perovskites.	11
Figure 1.6	Different types of organic photoredox reactions are carried out using halide perovskites.	13
Figure 1.7	Band edge positions of conventional photocatalysts and different MHPs relative to the reversible hydrogen electrode (NHE). For	14

comparison, the redox potential of some common half-reactions is also presented.

- Figure 1.8** Examples of the different types of drugs with amine and amide moieties. 18
- Figure 1.9** A diagram showing the chapter-wise specific objectives of the thesis. 21
- Figure 2.1** (a) PXRD pattern of monoclinic CsPbBr₃ QDs. (b) Crystal structure of monoclinic CsPbBr₃ QDs. (c) TEM image of CsPbBr₃ QDs with inset showing size distribution. (d) High-resolution TEM image highlighting crystal planes of monoclinic CsPbBr₃ QDs. (e) FFT (1–4) and corresponding inverse FFT (1'–4') images from the selected area in (d). (f) EDX spectrum confirming the presence of Cs, Pb, and Br elements. 37
- Figure 2.2** (a) Cyclic voltammogram of CsPbBr₃ QDs and 7% [Ni]-CsPbBr₃ in the dark and light. XPS spectra of CsPbBr₃ and 7% [Ni]-CsPbBr₃ (b) Cs 3d, (c) Pb 4f, (d) Br 3d. (e) Ni 2p XPS of 7% [Ni]-CsPbBr₃ showing the presence of Ni²⁺ species and inset figure (e') in figure (e), O 1s XPS of 7% [Ni]-CsPbBr₃ showing the presence of oxygen of adsorbed water (530.71 eV) and –OH group of the ligand of Ni(dmgh)₂ (532.23 eV). (f) C 1s XPS of 7% [Ni]-CsPbBr₃ showing C=O and C=C bonds at 287.64 eV and 285.59 eV, respectively, while the peak at 284.37 eV is associated with carbon and inset figure (f') in the figure (f), N 1s XPS of 7% [Ni]-CsPbBr₃ showing the peak for C=N bond (399.7 eV) and N-O species (402.34 eV). 38
- Figure 2.3** (a) Cyclic voltammograms of pristine CsPbBr₃ QDs and 7 wt.% [Ni]-CsPbBr₃ under dark and light conditions. High-resolution XPS spectra of CsPbBr₃ and 7 wt.% [Ni]-CsPbBr₃: (b) Cs 3d, (c) Pb 4f, (d) Br 3d. (e) Ni 2p spectrum of 7 wt.% [Ni]-CsPbBr₃ confirming the presence of Ni²⁺ species; inset (e') shows O 1s spectrum indicating adsorbed water (530.71 eV) and –OH groups from the Ni(dmgh)₂ ligand (532.23 eV). (f) C 1s spectrum displaying peaks corresponding to C=O (287.64 eV), C=C (285.59 eV), and adventitious carbon 39

- (284.37 eV); inset (f') shows N 1s spectrum with peaks attributed to C=N (399.7 eV) and N-O (402.34 eV) species.
- Figure 2.4** Transient absorption (TA) spectra were recorded at various pump-probe delay times for CsPbBr₃ (a–g) and 7% [Ni]-CsPbBr₃ (h–n). The spectral region between ~390 nm and 450 nm was amplified tenfold to enhance clarity. Each spectrum is labeled with its corresponding delay time. PB indicates photo-bleaching, while ESA refers to excited-state absorption. **46**
- Figure 2.5** (a) Kinetic profiles measured at (1) 400 nm, (2) 500 nm, (3) 550 nm, and (4) 650 nm for CsPbBr₃ (red) and 7% [Ni]-CsPbBr₃ (blue), with solid lines representing fitted curves. (b) Decay-associated spectra (DAS) of CsPbBr₃ and (c) 7% [Ni]-CsPbBr₃. (d) Schematic representation illustrating charge carrier generation and relaxation processes in CsPbBr₃ and 7% [Ni]-CsPbBr₃. (e) TA spectra of CsPbBr₃ and (f) TA spectra of 7% [Ni]-CsPbBr₃. **46**
- Figure 2.6** (a) Proposed mechanism of C–N bond formation under visible light. (b) Photocatalytic recyclability test for amide bond formation. (c) UV-vis spectra confirmed that the absorption peak did not change after 4 times recycling of 7%[Ni]-CsPbBr₃. **49**
- Figure 2.7** ((a) Quenching studies using various scavengers to identify reactive species involved in the process. (b) Identification of superoxide radicals generated through dioxygen reduction during photocatalysis. (c) Analysis of H₂O₂ formation resulting from photoredox reactions involving CsPbBr₃ and 7% [Ni]-CsPbBr₃. (d) Time-dependent detection of H₂O₂ produced during the photoredox reaction with 7% [Ni]-CsPbBr₃. **50**
- Figure 2.8** ¹H NMR and ¹³C NMR spectra of the compound 2h. **56**
- Figure 3.1** Molecular structures of ligands L1–L4, synthetic scheme of the [Co-4] complex, and the molecular structure of the resulting cobalt complex. **64**

- Figure 3.2** (a) The UV-DRS spectra of CsPbBr₃, CsPbBr₃-[Co-1], CsPbBr₃-[Co-2], CsPbBr₃-[Co-3], and CsPbBr₃-[Co-4], and the inset figure Tauc plot of all catalysts. (b) UV-visible spectra of the cocatalysts. (c) Photoluminescence spectra of CsPbBr₃ and others with cocatalysts. (d) Electrochemical impedance spectroscopic studies of bare CsPbBr₃ and with all the cocatalysts. (e) Photocurrent measurements of bare CsPbBr₃ and with all the cocatalysts under light/dark conditions. (f) Mott–Schottky measurements. **65**
- Figure 3.3** (a) N-alkylation activity over different photocatalysts with [Co-4]. (b) N-alkylation activity over CsPbBr₃ with different cocatalysts. (c) Quenching experiments. (d) The optimization of N-alkylation of aniline with benzylalcohol. (e) Proposed mechanism of N-alkylation reaction over CsPbBr₃-[Co-4] catalyst. **71**
- Figure 3.4** (a) The optimization rate of the dehydrogenation of benzylalcohol. (b) The selectivity of the N-alkylation reaction over all the catalysts. (c) Model reactions illustrating the strong hydrogen atom transfer ability of CsPbBr₃-[Co-4]. (d) Time-dependent reaction of N-alkylation of amine over CsPbBr₃-[Co-4]. (e) Recyclability test. (f) Comparison of UV-DRS before and after the photocatalyst. **73**
- Figure 3.5** ¹H NMR and ¹³C NMR spectra of the compound 3a. **80**
- Figure 4.1** Schematic representation of molecular oxygen activation and hole utilization with CsPbBr₃/BiOBr heterojunction photocatalyst (Z-20) for the semidehydrogenation of 1,2,3,4-tetrahydroisoquinoline. **86**
- Figure 4.2** (a) TEM image of Z-20 showing the deposition of CsPbBr₃ QDs on the surface of BiOBr nanosheets. CsPbBr₃ QDs on the surface of BiOBr are marked with circles. (b) HR-TEM confirmed the formation of heterojunction of QDs and BiOBr. (c,d) The lattices are 0.41 nm for CsPbBr₃ QDs and 0.27 nm for BiOBr, corresponding to (110) planes of both semiconductors. (c' and d') Selected area FFT showing **88**

the diffractions for CsPbBr₃ and BiOBr in Z-20. (c'' and d'') are the Inverse FFT of figures c' and d', respectively. (e-i) EDX elemental mapping of Z-20. (j) PXRD patterns of CsPbBr₃, BiOBr, and Z-20. (k) Cs 3d XP spectra of CsPbBr₃, and Z-20; (l) Pb 4f XP spectra of CsPbBr₃, and Z-20; and (m) Bi 4f XP spectra of BiOBr, and Z-20. (n) Br 3d XPS of Z-20, CsPbBr₃, and BiOBr. (o) O 1s XPS of Z-20 and BiOBr.

- Figure 4.3** (a) The UV-vis. diffuse reflectance spectra of CsPbBr₃ QDs, Z-20, and BiOBr, inset showing Tauc plot corresponding to figure (a), no significant change in the bandgap of CsPbBr₃ after the introduction of the CsPbBr₃ QDs to BiOBr nanosheets. (b, c) Mott-Schottky plots of CsPbBr₃ and BiOBr. (d, e) Valence band XPS of (d) CsPbBr₃ and (e) BiOBr. (f) Depiction of the conduction band minima and valence band maxima for CsPbBr₃ QDs and BiOBr NSs, derived from Tauc plot and Mott-Schottky studies. 90
- Figure 4.4** (a and b) UPS spectra showing the secondary electron cut-off for CsPbBr₃ and BiOBr photocatalysts were analyzed. The end energy levels (EEL) of CsPbBr₃ and BiOBr were measured as 17.02 eV and 15.21 eV, respectively. Using the Fermi level (E_F) and the equation $\Phi = 21.2 - EEL$, the work functions (Φ) of CsPbBr₃ and BiOBr were calculated to be 4.2 eV and 6.01 eV, respectively. (c) Schematic representation of BiOBr/CsPbBr₃ heterojunction: internal electric field (IEF) induced charge transfer, separation, and the formation of Z-scheme heterojunction under UV-Visible light irradiation for photocatalytic semidehydrogenation of THIQ. (d) ESR spectra of DMPO-O₂^{•-} and (e) DMPO-•OH. 91
- Figure 4.5** (a) Photocurrent of BiOBr, CsPbBr₃, and heterojunction Z-20 under light/dark conditions. (b) EIS of BiOBr, CsPbBr₃, and Z-20. (c) PL spectra of CsPbBr₃ and Z-20 at 370 nm excitation wavelength (Inset 96

image shows the PL spectra of BiOBr at 335 nm excitation wavelength). (d) TA spectra of CsPbBr₃, (e) TA spectra of Z-20. Kinetic traces for CsPbBr₃ (violet) and Z-20 (orange) at probe wavelengths (f) 490 nm (g) 500 nm (h) 550 nm, and (i) 600 nm, the solid lines are fitted lines. (j, k) the decay-associated spectra (DAS) of CsPbBr₃ and Z-20. (l) A schematic depiction of the formation and relaxation of charge carriers in CsPbBr₃ and Z-20.

- Figure 4.6** The transient absorption (TA) spectra at different delay times between pump and probe (a) CsPbBr₃, (b) Z-20. 97
- Figure 4.7** (a) Photocatalytic test with all catalysts. (b) Time-dependent conversion of 1,2,3,4-tetrahydroisoquinoline and DHIQ products formed with Z-20 heterojunction in air and light. After achieving the highest yield of DHIQ not convert into IQ with increasing reaction time. (c) Different heterostructure photocatalysts for semidehydrogenation of THIQ in air. (d) Proposed mechanism of semidehydrogenation of THIQ. (e) Detection of photogenerated superoxide radicals (NBT test). (f) ¹O₂ radical trapping by EPR spectroscopy. 102
- Figure 4.8** (a) UV-visible spectroscopy detects the photogenerated ¹O₂. (b) ¹O₂ generation through the reaction ($O_2^{\bullet-} + h^+ \rightarrow {}^1O_2$) process. (c) UV-visible spectroscopy detects the photogenerated H₂O₂ in the reaction mixture over CsPbBr₃, BiOBr, and Z-20 catalysts. (d) Quenching experiments. (e) Recyclability of Z-20 photocatalyst for semidehydrogenation of THIQ in air. (f) UV-vis-DRS of Z-20 after five cycles in air. 103
- Figure 4.9** ¹H NMR and ¹³C NMR spectra of separated DHIQ in CDCl₃. 105
- Scheme 5.1** Schematic representation showing the structural modulation of Cs₂CuBr₄ by two different synthesis methods: (i) Hot-injection (PC-1) and (ii) Room temperature (PC-2). 110
- Figure 5.1** (a) PXRD patterns of PC-1 and PC-2 matched with JCPDS no. 71-1462. (b and c) SEM image showing the rod shape morphology of PC- 112

- 1 and PC-2; (d) TEM image of PC-1, showing nanorod morphology. (e) High-resolution TEM image showing the lattice spacing corresponding to the (203) plane of Cs_2CuBr_4 . (f) Fast Fourier transform (FFT) and (g) inverse FFT corresponding to the selected circle area of (e). (H and i) Elemental mapping of PC-1 and PC-2 showing the uniform distribution of Cs, Cu, and Br.
- Figure 5.2** Comparison of XPS of PC-1 and PC-2, showing in figure (a) Cs 3d, (b) Cu 2p, (c) Br 3d. XPS of Cs, Cu, and Br showed a positive shift of the peaks in PC-1 compared to PC-2 because of the structural modulation. **113**
- Figure 5.3** (a) The UV-vis. diffuse reflectance spectra of PC-1 and PC-2, inset showing the corresponding Tauc plot, demonstrating a significant change in the band gap for PC-1 and PC-2. (b and c) Mott-Schottky plot of PC-1 and PC-2. (d) The conduction band minima and valence band maxima for PC-1 and PC-2, derived from Tauc plot and Mott-Schottky studies. **114**
- Figure 5.4** (a) Differential pulse voltammograms (DPV) of PC-1 and PC-2 were recorded under dark and illuminated conditions. (b) Photoluminescence spectra indicating reduced charge carrier recombination in PC-1 compared to PC-2. (c) Transient photocurrent responses under light/dark cycles, demonstrating enhanced charge separation efficiency in PC-1. (d) Electrochemical impedance spectra under illumination, showing lower charge transfer resistance for PC-1 relative to PC-2. **115**
- Figure 5.5** (a) The proposed mechanism for photocatalytic oxidative amidation of alcohol is based on the detected intermediates. (b) Difference in the rate of the reactions for C–N bond formation. (c) Quenching experiments confirmed the radical process involved in the amide bond formation reaction. **121**
- Figure 5.6** (a) Detection of photogenerated superoxide radicals. (b) UV-visible spectroscopic detection of photogenerated H_2O_2 in the reaction **122**

mixture. (c) Recyclability of PC-1 photocatalyst for amide bond formation reaction. (d) UV-vis-DRS of PC-1 after five cycles and before catalysis

Figure 5.7 ^1H NMR and ^{13}C NMR spectra of the compound 5c.

126

List of Table

Table No.	Title	Page No.
Table 2.1	Description of the catalyst	34
Table 2.2	Optimization of photoredox C–N coupling reaction conditions	43
Table 2.3	Photocatalytic C–N bond formation in the presence of visible light using 7% [Ni]-CsPbBr ₃ photocatalyst.	45
Table 2.4	Characterization of the products by ¹ H NMR and ¹³ C NMR spectroscopy ⁷	52
Table 3.1	Description of the photocatalyst systems.	65
Table 3.2	Optimization of <i>N</i> -alkylation of aniline with benzyl alcohol under different conditions	69
Table 3.3	The substrate scope of <i>N</i> -alkylation of amines.	76
Table 3.4	Characterization of the products by ¹ H NMR and ¹³ C NMR spectroscopy	77
Table 4.1	Description of the photocatalysts	
Table 4.2	Fitting coefficient of kinetics traces at 490nm, 500 nm, 550 nm and 600 nm of CsPbBr ₃ and Z-20 excited state at 370 nm	97
Table 4.3	Photocatalytic optimization conditions of semi-dehydrogenation of 1,2,3,4-Tetrahydroisoquinoline	99
Table 5.1	Description of the photocatalysts	111
Table 5.2	Comparison of the photocatalytic activities of PC-1 and PC-2 for the amidation of alcohols in the presence of light	117
Table 5.3	Optimization of the reaction conditions for photocatalytic amination of alcohols.	118
Table 5.4	The substrate scope of different alcohols and amines for amide bond formation.	119
Table 5.5	¹ H NMR and ¹³ C NMR spectra of the products	123

List of Symbols/Abbreviations

θ	Angle (degree)
τ	Trap-state
a.u.	Atomic unit
BE	Binding energy
CBM	Conduction band maxima
¹³C NMR	Carbon nuclear magnetic resonance
eV	Electron volt
EIS	Electrochemical impedance spectroscopy
EDX	Energy-dispersive X-ray spectroscopy
EPR	Electron spin resonance
Fs-TA	Femtosecond transient spectroscopy
HR-SEM	High Resolution Scanning Electron Microscope
¹H NMR	Hydrogen nuclear magnetic resonance
HR-MS	High-resolution mass spectroscopy
mM	Milli-molar
NS	Nanosheet
NHE	Normal hydrogen electrode
PL	Photoluminescence
PXRD	Powder X-ray diffraction
TEM	Transmission Electron Microscopy
XPS	X-ray photoelectron spectroscopy
UV-DRS	Ultraviolet diffused reflectance spectroscopy
UPS	Ultraviolet photoelectron spectroscopy
VBM	Valence band minima
QDs	Quantum dots
λ	Wavelength